Optica Applicata, Vol. LIV, No. 4, 2024
DOI: 10.37190/oa/195221

Multi-focus auto focusing characteristics of vector beam with non-uniformly correlated structure in a turbulent atmosphere

Xianyang Yang[1], Wenyu Fu[2,*], Xiaolu Zhu[3]

[1] School of Intelligent Manufacturing and Energy Engineering, Jiang-Xi University of Engineering, Xinyu, 33800, Jiangxi, China

[2] College of Electronic Information Engineering, Jiang-Xi University of Engineering, Xinyu, 33800, Jiangxi, China

[3] School of New Energy, Longdong University, Qingyang, 74500, Gansu, China

[*] Corresponding author: qytcfwy@163.com

We propose a simple strategy to produce multiple longitudinal focal spots by adjusting the initial parameters of vector beam with non-uniformly correlated structure and chose electromagnetic Hermite non-uniformly correlated (EMHNUC) beams as typical examples to explore the multi-focusing characteristics of the beam propagation in turbulent atmosphere. Furthermore, we also demonstrated how to control the foci's number, intensity, and position by adjusting the vector beam's initial parameters. Finally, the influence of the turbulent atmosphere on the focal spot intensity was analyzed. These beams may prove helpful in longitudinal optical trapping and manipulation of multiple particles and transparent material cutting.

Keywords: electromagnetic Hermite non-uniformly beams, multi-focusing characteristics, turbulent atmosphere.

1. Introduction

Light beams whose spatial dimension parameters are modulated to produce a new light field with a specific distribution are called spatially structured light beams. Compared to the first-order statistical parameters such as amplitude, phase, and polarization state of a random light field, coherent structures, as second-order statistical parameters of beams, are unique degrees of freedom for coherent beams and partially coherent beams, exhibiting many novel physical properties in their control, and has found use in constructing new structured light beams and a wide range of applications [1-2]. In recent years, partially coherent beams based on coherent structure control have attracted widespread attention due to their unique advantages in resisting the adverse effects of turbulence, self-healing solid ability, and overcoming speckle noise [3-7].

Since a new method for designing novel correlation functions of scalar and vector partially coherent beams was discussed by GORI *et al*. [8,9], a great deal of research has been done on designing various partially coherent structured beams with prescribed spatial coherence [10]; this enables a host of applications [11], including ghost imaging [12] and partially coherent diffractive imaging [13]. In 2011, LAJUNEN *et al*. introduced a new class of partially coherent beams with a spatially variant correlation function (*i.e.*, non-uniformly correlated beams) [14]. Their new class exhibited self -focusing and self-shifting propagation properties, which provides a new research approach for applications such as optical capture and particle manipulation [15]. In later years, researchers successively introduced non-uniform Laguerre Gaussian correlated beams, non-uniform correlated Bessel beams, pseudo-Bessel correlated beams, Hermite non-uniformly correlated beams, radially polarized Hermite non-uniformly correlated beams, *etc*. [16-20], which significantly deepens the research on non-uniform correlated beams.

Recently, a multi-focus beam with a spatial non-uniform coherence structure was introduced, which exhibits multiple longitudinal focal spots on propagation. Compared to the previous works [21], such low-coherence beams achieve a multi-focal effect and avoid the adverse effects caused by high coherence. However, this research was obtained within the scalar approximation, which overlooks the polarization properties of vector beams; it is expected that, as non-uniformly correlated beams have shown advantages in optical applications, the vector beam introduced by the combination of polarization and non-uniform coherence leads to the discovery of new effects.

In this paper, we propose a simple strategy to produce multiple longitudinal focal spots by adjusting the initial parameters of vector beam with non-uniformly correlated structure, and we choose electromagnetic Hermite non-uniformly correlated (EMHNUC) beams as typical examples to explore the multi-focusing characteristics of the beam propagation in turbulent atmosphere. Furthermore, we also demonstrated how to control the foci's number, intensity, and position by adjusting the vector beam's initial parameters.

2. EMHNUC source

Usually, the spatial coherence characteristics of vector partially coherent beams are characterized by the cross-spectral density (CSD) matrix in the spatial frequency domain. The CSD matrix of quasi-monochromatic fields at two position vectors ρ_1 and ρ_2 in the source plane is defined as [22]

$$W_{\alpha\beta}(\rho_1, \rho_2) = \langle E_\alpha^*(\rho_1) E_\beta(\rho_2) \rangle, \quad (\alpha, \beta = x, y) \tag{1}$$

In Eq. (1), the symbols E_x and E_y represent the two mutually orthogonal components of the random electric vector along the x and y axes, respectively, which are mutually orthogonal to the z axis. The asterisk denotes the complex conjugate, and the angular brackets denote an average over a monochromatic ensemble.

From the reports of GORI *et al.* [9], it is known that any CSD matrix expressed in the following one-dimensional integral form is physically realizable.

$$W_{\alpha\beta}(\rho_1, \rho_2) = \int p_{\alpha\beta}(v)\, h_\alpha^*(\rho_1, v)\, h_\beta(\rho_2, v)\, \mathrm{d}v \tag{2}$$

where $h_\alpha(\rho_1, v)$ and $h_\beta(\rho_2, v)$ represent arbitrary kernel functions, v denotes a one-dimensional vector, $p_{\alpha\beta}(v)$ are the elements of the weighting matrix, and the elements of the weighting matrix must satisfy the following inequalities

$$p_{xx}(v) \geq 0 \tag{3a}$$

$$p_{yy}(v) \geq 0 \tag{3b}$$

$$p_{xx}(v)\, p_{yy}(v) - p_{xy}(v)\, p_{yx}(v) \geq 0 \tag{3c}$$

here, we take $h_{\alpha(\beta)}(\rho, v)$ and $p_{\alpha\beta}(v)$ to the form, respectively

$$h_\alpha(\rho, v) = A_\alpha \exp\left(-\frac{x^2}{2w_{0x}^2} - \frac{y^2}{2w_{0y}^2}\right) \exp(-ikv\rho^2) \tag{4}$$

$$p_{\alpha\beta}(v) = B_{\alpha\beta}(\pi a_{\alpha\beta}^2)^{-1} \left(\frac{2v}{a_{\alpha\beta}^2}\right)^{2n} \exp\left(-\frac{v^2}{a_{\alpha\beta}^2}\right) \tag{5}$$

where the beam width is denoted by w_{0x} and w_{0y}, respectively, A_α represents the amplitudes of the electric field component along the α direction, $B_{\alpha\beta}$ is the complex correlation coefficient. Substituting Eqs. (4) and (5) into Eq. (2) we derive the CSD of EMHNUC beams as the following expression

$$\begin{aligned} W_{\alpha\beta}(\rho_1, \rho_2) &= G_0 A_\alpha A_\beta B_{\alpha\beta} \exp\left(-\frac{x_1^2 + x_2^2}{2w_{0x}^2} - \frac{y_1^2 + y_2^2}{2w_{0y}^2}\right) \\ &\times \exp\left[-\frac{(\rho_1^2 - \rho_2^2)^2}{r_{\alpha\beta}^4}\right] H_{2n}\left(\frac{\rho_1^2 - \rho_2^2}{r_{\alpha\beta}^2}\right) \end{aligned} \tag{6}$$

where $r_{\alpha\beta} = (2/ka_{\alpha\beta})^{1/2}$ is the correlation width, $H_{2n}(\cdot)$ denotes the Hermite polynomials order $2n$, $G_0 = 1/H_{2n}(0)$, and $B_{\alpha\beta}$ is the maximum correlation between the E_α and E_β field components. In the following, let us concentrate our attention on the paraxial propagation of this beam through turbulent atmosphere. The CSD matrix elements of the EMHNUC beams can be obtained using the following expression [11]

$$W_{\alpha\beta}(r_1, r_2, z) = \left(\frac{k}{2\pi z}\right)^2 \iint \left\{ \begin{array}{c} W_{\alpha\beta}(\rho_1, \rho_2) \exp\left[-ik \dfrac{(r_1-\rho_1)^2 - (r_2-\rho_2)^2}{2z}\right] \\ \times \langle \exp[\psi(r_1, \rho_1) + \psi^*(r_2, \rho_2)] \rangle_{\mathrm{R}} \end{array} \right\} \mathrm{d}^2\rho_1 \, \mathrm{d}^2\rho_2 \tag{7}$$

where ψ stands for the complex phase perturbation caused by the medium, $\langle\cdot\rangle_{\mathrm{R}}$ implying averaging over the ensemble of statistical realizations of the turbulence. Under quadratic phase approximations, $\langle\cdot\rangle_{\mathrm{R}}$ can be rewritten as

$$\langle \exp[\psi(r_1, \rho_1) + \psi^*(r_2, \rho_2)] \rangle_{\mathrm{R}} = \exp\left\{ -\frac{\pi^2 k^2 z}{3} \int_0^\infty \kappa^3 \varphi_n(\kappa) \mathrm{d}\kappa \left[(r_1 - r_2)^2 + (r_1 - r_2)(\rho_1 - \rho_2) + (\rho_1 - \rho_2)^2 \right] \right\} \tag{8}$$

here, we select the van Karman power spectrum to represent the an-isotropic characteristics of the atmosphere [4, 17], where κ represents the magnitude of the spatial wave number.

$$\Phi_n(\kappa) = 0.033\, C_n^2 (\kappa^2 + \kappa_0^2)^{-11/6} \exp(\kappa^2/\kappa_{\mathrm{m}}) \tag{9}$$

where C_n^2 represents a generalized refractive-index structure parameter, $\kappa_0 = 2\pi/L_0$ and $\kappa_{\mathrm{m}} = 592/l_0$ with L_0 and l_0 represent parameters associated with the outer scale L_0 and inner scale l_0 of turbulence, respectively. By substituting Eqs. (8) and (2) into Eq. (7) with some algebraic transformations and integral operations, we obtained a general expression of CSD matrix elements of the EMHNUC beams in turbulence.

$$W_{\alpha\beta}(r, r, z) = A_\alpha A_\beta B_{\alpha\beta} \int \frac{w_{0x} w_{0y} p_{\alpha\beta}(v)}{w_x(v, z) w_y(v, z)} \exp\left[-\left(\frac{x^2}{w_x(v, z)} + \frac{y^2}{w_y(v, z)}\right)\right] \mathrm{d}v \tag{10}$$

Similarly, the spectral intensity of the non-uniformly correlated beams can be written as [22]

$$S(r, z) = \mathrm{Tr}\left[W(r, r, z)\right] = W_{xx}(r, r, z) + W_{yy}(r, r, z) \tag{11}$$

where

$$w_\alpha(v, z) = \frac{w_{0\alpha}^2(1-2vz)^2}{2} + \frac{2z^2}{k^2 w_{0\alpha}^2} + \frac{4zT(z)}{k}, \quad (\alpha = x, y) \tag{12}$$

$$T(z) = \frac{\pi^2 k^2 z}{3}\int_0^\infty \kappa^3 \varphi_n(\kappa)\,\mathrm{d}\kappa \tag{13}$$

the degree of polarization (DOP) of the EMHNUC beams can be expressed as

$$P(r, z) = \sqrt{1 - \frac{4\,\mathrm{Det}\left[W(r, r, z)\right]}{\mathrm{Tr}(r, r, z)^2}} \tag{14}$$

where Tr and Det represent the determinant and trace of the CSD matrix, for the convenience of the following analysis, we set the ratio of field amplitude $e = A_y/A_x$. The state of polarization (SOP) of the EMHNUC beams can be characterized by polarization ellipse, orientation angle, and its degree of ellipticity are related to the elements of the CSD matrix $W_{\alpha\beta}(r, r)$ by the following relations as described in [23].

3. Numerical simulation and analysis

Next, we explore the propagation characteristics of EMHNUC beams under different light source parameters and turbulent parameters. In the following calculations, we assume that $A_y = 1$, $B_{xx} = B_{yy} = 1$, $B_{xy} = 0.5\exp(\pi/4)$, $\lambda = 632.8$ nm, $w_{0x} = 3$ cm, $w_{0y} = 3$ cm, $r_{xx} = 2$ cm, $r_{yy} = 2$ cm, $r_{xy} = 2$ cm, $n = 1$, $e = 0.5$, $L_0 = 1$ m, $l_0 = 1$ mm and $C_n^2 = 10^{-15}$ m$^{-2/3}$ unless otherwise indicated in figures. Figure 1 illustrates the normalized intensity distribution of EMHNUC beams at different distances with different beam source parameters. It is observed that the beam spot does not diverge monotonically but exhibits a clear self-focusing phenomenon during propagation. Due to the consistent coherence length and beam width of the two perpendicular components of the vector beam, the intensity of EMHNUC beams exhibits a symmetrical distribution. As the propagation distance increases, the light intensity distribution shrinks, enlarges, and then shrinks again, resulting in a significant self-focusing phenomenon (as shown in Fig. 1(a)). When the two coherent length components and beam width components are not the same, the two-component beams exhibit self-focusing, and the positions of their respective focal spots deviate along the propagation direction, which results in the secondary focusing phenomenon (as shown in Fig. 1(b)-(c)). From Fig. 1(d), it can be seen that the higher the order of the beam, the smaller and brighter the two focal points, indicating that the self-focusing of the beam is more significant. The secondary self-focusing of EMHNUC beams comes from their unique, coherent structure. The non-uni-

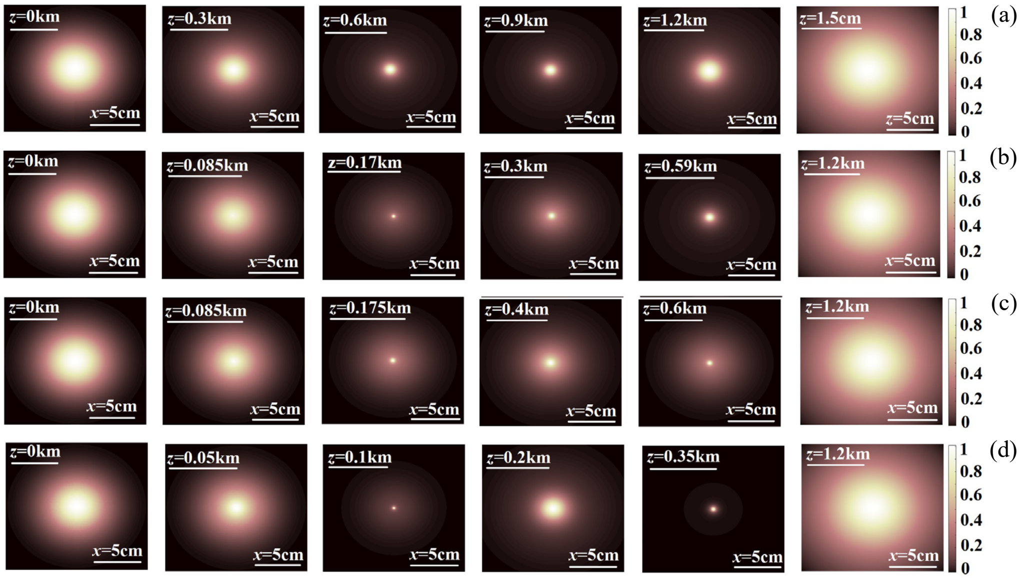

Fig. 1. Normalized intensity of the EMHNUC beams at different distances with different beam source parameters. (a) $w_{0x} = w_{0y} = 3$ cm, $r_{xx} = r_{yy} = 2$ cm; (b) $w_{0x} = w_{0y} = 3$ cm, $r_{xx} = 2$ cm, $r_{yy} = 1$ cm; (c) $w_{0x} = 3$ cm, $w_{0y} = 2$ cm, $r_{xx} = 2$ cm, $r_{yy} = 1$ cm; (d) $w_{0x} = 3$ cm, $w_{0y} = 2$ cm, $r_{xx} = 2$ cm, $r_{yy} = 1$ cm, $n = 3$.

formity coherent structure causes self-focusing of the beams during beam propagation, while the asymmetry coherence length is the reason for the secondary self-focusing of the beams. Accordingly, we can infer that combining the EMHNUC beams with different coherence lengths can generate multi-focusing points along the propagation direction, which can be used in longitudinal multi-particle optical trapping and transparent material cutting.

To further explore the longitudinal focusing characteristics of the EMHNUC beams, Fig. 2 shows the intensity distribution of the EMHNUC beams along the propagation direction z-axis in the xoz plane (see Fig. 2(a1)-(a4)) and the on-axis intensity distribution (see Fig. 2(b1)-(b4)) with different beam source parameters. When the coherence length and beam width of the two orthogonal components of the EMHNUC beam are the same due to the self-focusing characteristics of each element, the light intensity shows a precise longitudinal focusing distribution along the z-axis (as shown in Fig. 2(a1)-(b1)). As the coherence length and beam width of the beam components differ, the secondary longitudinal focusing distribution of the light intensity along the z-axis gradually becomes apparent, and the brightness of the focusing spot increases (as shown in Fig. 2(a2)-(a3) and (b2)-(b3)). Moreover, the focusing spot shortens significantly along the axis as the beam order increases. It exhibits unique longitudinal focusing characteristics (as shown in Fig. 2(a4)-(b4)).

Figure 3 shows the polarization properties of the EMHNUC beam with the same parameter as in Fig. 1(d) in a turbulent atmosphere. Figure 3(a) illustrates the evolution of the DOP of the EMHNUC beam, and Fig. 3(b) shows its corresponding distribution

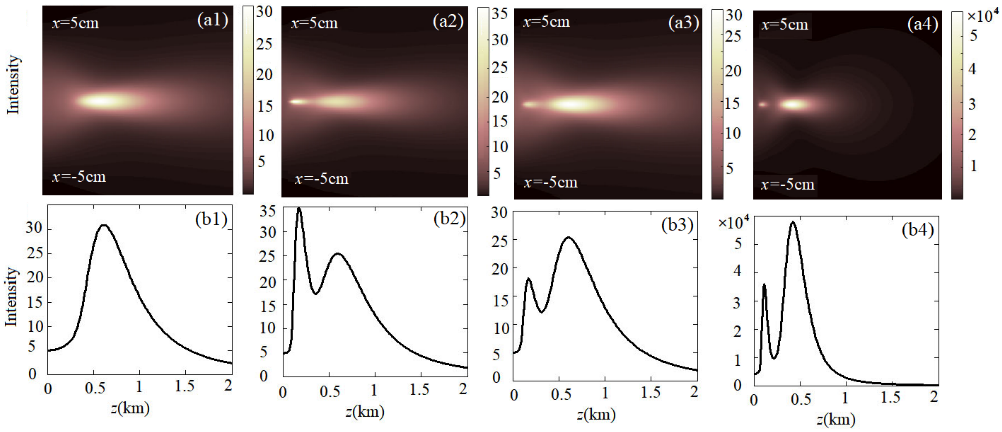

Fig. 2. Intensity distribution of the EMHNUC beam along the *z*-axis distance. The parameter selection from left to right is the same as the parameter selection in (a)-(d) in Fig. 1. (a) Intensity distribution of *xoz* plane. (b) On-axis intensity distribution along the *z*-axis.

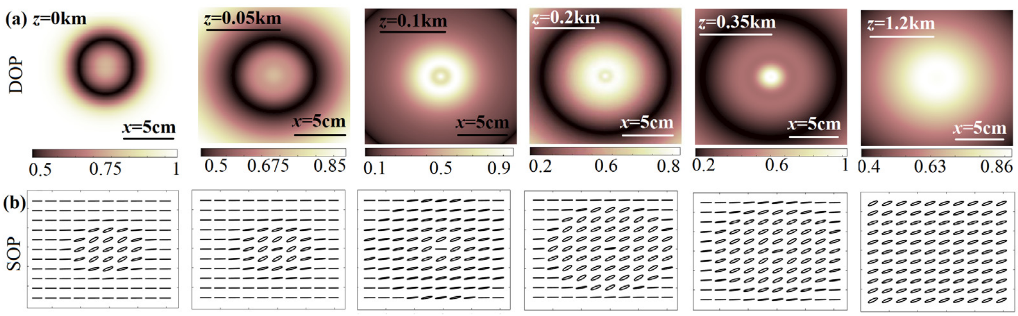

Fig. 3. Evolution of polarization characteristics of the EMHNUC beams in turbulence with (a) distribution of the DOP, and (b) distribution of the SOP. The parameter choices of the EMHNUC beams are the same as in Fig. 1(d).

of the SOP. It can be seen from Fig. 3, that due to its particular non-uniform coherent structure, the DOP of the EMHNUC beams has an axisymmetric non-uniform distribution, which also changes with the propagation distance (as shown in Fig. 3(a)). The SOP of the EMHNUC beams initially presents an elliptical polarization state distribution in the central region, surrounded by a linear polarization state distribution. As the propagation distance increases, the elliptical polarization distribution extends outward from the central region, and the entire distribution area shows a stable elliptical polarization state distribution.

Figure 4 explores how the number and position of focal points of the beam change as it propagates, based on different initial beam parameters. It is observed that the beam widths, coherence lengths, and beam order n mainly determine the number and position of the focal points (as shown in Fig. 4(a)-(c)). One can find from Fig. 4(a)-(b) that as the beam widths w_x (or w_y) and coherence lengths r_{cx} (or r_{cy}) change, the axial intensity

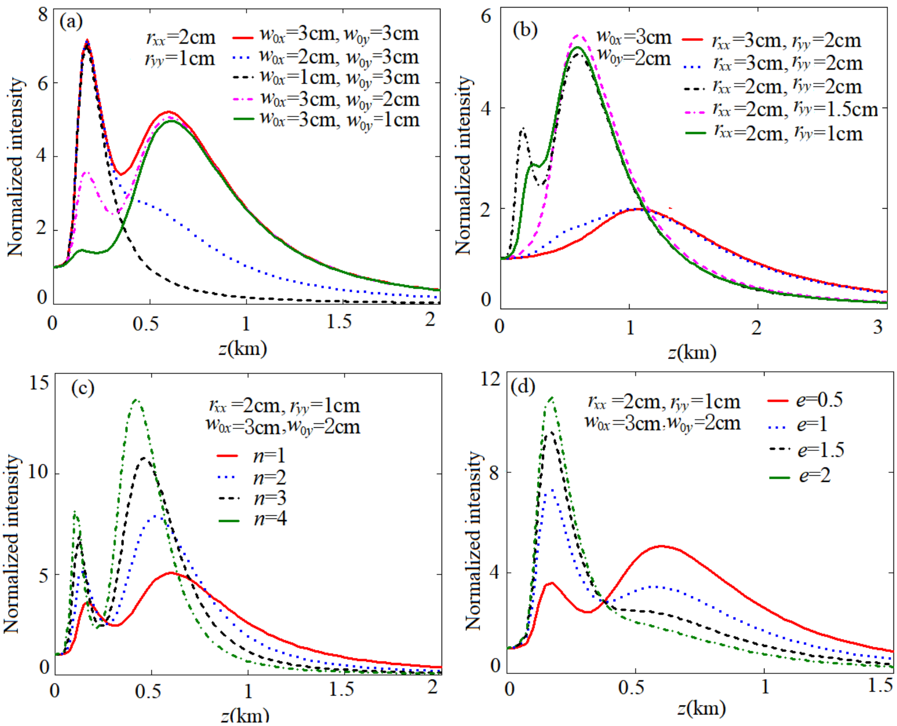

Fig. 4. On-axis distribution of normalized intensity of the EMHNUC beams for varying initial beam parameters and turbulence parameters. (a) For different w_{0x} and w_{0y}; (b) for different r_{xx} and r_{yy}; (c) for different n; (d) for different e in a turbulent atmosphere.

distribution also changes, thereby affecting the number and position of the beam's focal points. Figure 4(c) shows that the beam order n not only changes the position of the peak intensity but also affects its height. One also confirms from Fig. 4(d) that a change of the ratio of the field amplitude e will affect the height of the peak intensity distribution.

Next, we will discuss the influence of beam order n and amplitude ratio e on the size of the focal spot. Figure 5 shows the evolution of the intensity of the EMHNUC beams at different positions. One can find from Fig. 5(a)-(b) that as the amplitude ratio e and beam order n increase, the intensity distribution of the beam gradually expands outward, the expansion at the first position (z = 0.175 km) is more significant than that at the second position (z = 0.6 km), indicating that the focal spot becomes larger and the focusing effect weakens. Under the same conditions, the focusing effect at the second focal point is better than at the first.

To analyze the influence of turbulence parameters on the self-focusing of the beam further, Fig. 6 presents the intensity distribution of EMHNUC beams at different turbulent parameters. We can find from Fig. 6(a) that as the refractive-index structure parameter increases, the light intensity rapidly weakens, and the second peak gradually disappears, indicating that the refractive-index structure parameter has a significant im-

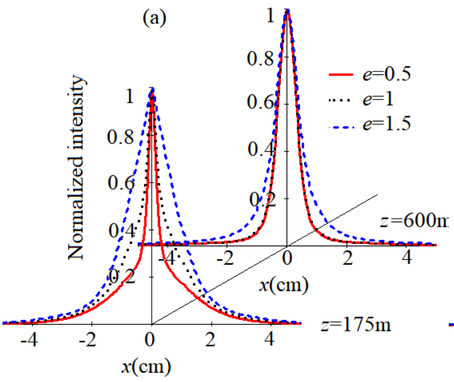

Fig. 5. Normalized intensity of EMHNUC beams at different positions with $w_{0x} = 3$ cm, $w_{0y} = 2$ cm, $r_{xx} = 2$ cm, and $r_{yy} = 1$ cm.

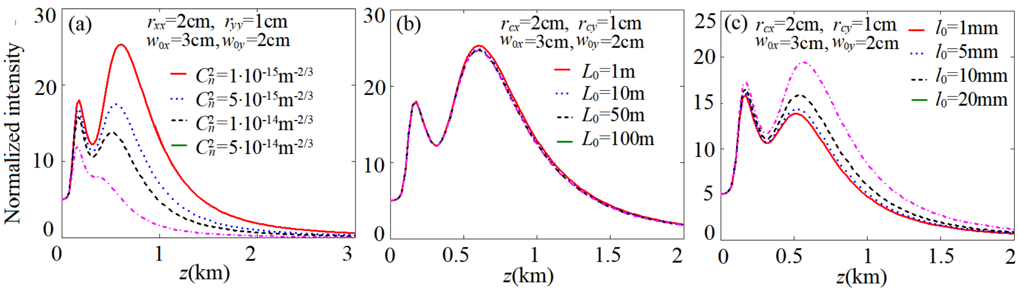

Fig. 6. Normalized intensity of EMHNUC beams at different turbulent parameters with $w_{0x} = 3$ cm, $w_{0y} = 2$ cm, $r_{xx} = 2$ cm, and $r_{yy} = 1$ cm.

pact on the multi-focus auto-focusing of the beam. Meanwhile, we also found that, compared to the inner scale l_0 (as shown in Fig. 6(c)), the influence of the outer scale L_0 on the on-axis intensity distribution of the beam is much weaker (as shown in Fig. 6(b)).

4. Conclusion

In this work, we choose electromagnetic Hermite non-uniformly correlated (EMHNUC) beams as typical examples to explore the multi-focus auto-focusing characteristics of vector beams with non-uniformly correlated structures. We also demonstrated controlling the number, intensity, and position by adjusting the vector beam's initial parameters. Furthermore, the effects of turbulence parameters on the self-focusing property of the beam are analyzed in detail. These results can be used in longitudinal multi-particle optical trapping and transparent material cutting.

Funding
National Science Foundation of China (12265018).

Conflict of interest

The authors declare no conflict of interest.

References

[1] GBUR G., *Partially coherent beam propagation in atmospheric turbulence*, Journal of the Optical Society of America A **31**(9), 2014: 2038-2045. https://doi.org/10.1364/JOSAA.31.002038

[2] CAI Y., CHEN Y., WANG F., *Generation and propagation of partially coherent beams with nonconventional correlation functions: A review*, Journal of the Optical Society of America A **31**(9), 2014: 2083-2096. https://doi.org/10.1364/JOSAA.31.002083

[3] PENG D., HUANG Z., LIU Y., CHEN Y., WANG F., PONOMARENKO S.A., CAI Y., *Optical coherence encryption with structured random light*, PhotoniX **2**, 2021: 6. https://doi.org/10.1186/s43074-021-00027-z

[4] KOROTKOVA O., ANDREWS L.C., PHILLIPS R.L., *Model for a partially coherent Gaussian beam in atmospheric turbulence with application in Lasercom*, Optical Engineering **43**(2), 2004: 330-341. https://doi.org/10.1117/1.1636185

[5] BOUCHAL Z., WAGNER J., CHLUP M., *Self-reconstruction of a distorted nondiffracting beam*, Optics Communications **151**(4-6), 1998: 207-211. https://doi.org/10.1016/S0030-4018(98)00085-6

[6] OTTE E., BOBKOVA V., TRINSCHEK S., ROSALES-GUZMÁN C., DENZ C., *Single-shot all-digital approach for measuring the orbital angular momentum spectrum of light*, APL Photonics **7**(8), 2022: 086105. https://doi.org/10.1063/5.0086536

[7] LIU Y., DONG Z., CHEN Y., CAI Y., *Research advances of partially coherent beams with novel coherence structures: Engineering and applications*, Opto-Electronic Engineering **49**(11), 2022: 220178. https://doi.org/10.12086/oee.2022.220178

[8] GORI F., SANTARSIERO M., *Devising genuine spatial correlation functions*, Optics Letters **32**(24), 2007: 3531-3533. https://doi.org/10.1364/OL.32.003531

[9] GORI F., RAMÍREZ-SÁNCHEZ V., SANTARSIERO M., SHIRAI T., *On genuine cross-spectral density matrices*, Journal of Optics A: Pure and Applied Optics **11**(8), 2009: 085706. https://doi.org/10.1088/1464-4258/11/8/085706

[10] CHEN Y., WANG F., CAI Y., *Partially coherent light beam shaping via complex spatial coherence structure engineering*, Advances in Physics: X **7**(1), 2022: 2009742. https://doi.org/10.1080/23746149.2021.2009742

[11] KOROTKOVA O., GBUR G., *Chapter Four - Applications of optical coherence theory*, [In:] *Progress in Optics*, [Ed.] T.D. Visser, Vol. 65, Elsevier, 2020: 43-104. https://doi.org/10.1016/bs.po.2019.11.004

[12] ZHOU Y., WU G., CAI Y., WANG F., HOENDERS B.J., *Application of self-healing property of partially coherent beams to ghost imaging*, Applied Physics Letters **117**(17), 2020: 171104. https://doi.org/10.1063/5.0025712

[13] LU X., SHAO Y., ZHAO C., KONIJNENBERG S., ZHU X., TANG Y., CAI Y., URBACH H.P., *Noniterative spatially partially coherent diffractive imaging using pinhole array mask*, Advanced Photonics **1**(1), 2019: 016005. https://doi.org/10.1117/1.AP.1.1.016005

[14] LAJUNEN H., SAASTAMOINEN T., *Propagation characteristics of partially coherent beams with spatially varying correlations*, Optics Letters **36**(20), 2011: 4104-4106. https://doi.org/10.1364/OL.36.004104

[15] YU J., XU Y., LIN S., ZHU X., GBUR G., CAI Y., *Longitudinal optical trapping and manipulating Rayleigh particles by spatial nonuniform coherence engineering*, Physical Review A **106**(3), 2022: 033511. https://doi.org/10.1103/PhysRevA.106.033511

[16] WU D., WANG F., CAI Y., *High-order nonuniformly correlated beams*, Optics & Laser Technology **99**, 2018: 230-237. https://doi.org/10.1016/j.optlastec.2017.09.007

[17] GU Y., GBUR G., *Scintillation of pseudo-Bessel correlated beams in atmospheric turbulence*, Journal of the Optical Society of America A **27**(12), 2010: 2621-2629. https://doi.org/10.1364/JOSAA.27.002621

[18] SONG Z., LIU Z., ZHOU K., SUN Q., LIU S., *Propagation characteristics of a non-uniformly Hermite –Gaussian correlated beam*, Journal of Optics **18**(1), 2016: 015606. https://doi.org/10.1088/2040-8978/18/1/015606

[19] LIN S., WANG C., ZHU X., LIN R., WANG F., GBUR G., CAI Y., YU J., *Propagation of radially polarized Hermite non-uniformly correlated beams in a turbulent atmosphere*, Optics Express **28**(19), 2020: 27238-27249. https://doi.org/10.1364/OE.402021

[20] YANG X., FU W., *Propagation of radially polarized beams with a Hermite non-uniformly correlated array in free space and turbulent atmosphere*, Optics Express **31**(9), 2023: 14403-14413. https://doi.org/10.1364/OE.486599

[21] XU Y., GUAN Y., LIU Y., LIN S., ZHU X., CAI Y., YU J., GBUR G., *Generating multi-focus beams with a spatial non-uniform coherence structure*, Optics Letters **48**(10), 2023: 2631-2634. https://doi.org/10.1364/OL.491880

[22] MEYSTRE P., *Introduction to the theory of coherence and polarization of light*, Physics Today **61**(12), 2008: 59-60. https://doi.org/10.1063/1.3047693

[23] AL-QASIMI A., KOROTKOVA O., JAMES D., WOLF E., *Definitions of the degree of polarization of a light beam*, Optics Letters **32**(9), 2007: 1015-1016. https://doi.org/10.1364/OL.32.001015

Received July 5, 2024
in revised form October 18, 2024